applied sciences

MDPI

Article

High-Speed Alumina Stereolithography

Fiona Spirrett *, Tatsuya Ito and Soshu Kirihara

Joining and Welding Research Institute, Osaka University, Osaka 567-0047, Japan
* Correspondence: fiona-spirrett@jwri.osaka-u.ac.jp

Abstract: The additive manufacturing of ceramics offers a reliable and repeatable method for fabricating parts with complex geometries. To compete with conventional ceramic forming methods, the time and cost associated with material and process optimization for ceramic stereolithography should be improved. Computational analysis methods can be utilized to reduce the number of experimental steps required for material and process optimization. This work used the discrete element method and ray tracing analyses to predict suitable material parameters and processing conditions for ceramic stereolithography. The discrete element method was used to create alumina particle dispersion models to predict suitable paste compositions, and ray tracing was used to predict suitable laser power and scan speed to achieve a sufficient curing depth for stereolithography processing. The predicted conditions of paste composition and processing parameters were comparable to experimental values, reducing the number of experimental iterations required for process optimization. Furthermore, suitable processing parameters for high-speed fabrication by stereolithography was predicted, achieving a processing speed much faster than previously reported ceramic stereolithography. The reduction in process optimization timeline, and the increase in fabrication speed, could increase the appeal of ceramic stereolithography to industry.

Keywords: discrete element method; ray tracing; stereolithography; alumina; additive manufacturing; ceramics

Citation: Spirrett, F.; Ito, T.; Kirihara, S. High-Speed Alumina Stereolithography. *Appl. Sci.* **2022**, *12*, 9760. https://doi.org/10.3390/app12199760

Academic Editors: Abílio Manuel Pinho de Jesus and Joamin Gonzalez-Gutierrez

Received: 18 August 2022
Accepted: 26 September 2022
Published: 28 September 2022

1. Introduction

In recent years, sustainability has become a significant concern in the manufacturing industry. Additive manufacturing describes a group of processes that fabricate 3D parts by the layer-wise joining of material from 3D model data [1]. In general, additive manufacturing (AM) technologies have many environmental benefits over conventional manufacturing, that have further driven innovation in the field. By using additive techniques, material waste can be reduced, new and smart materials can be used, and parts can be manufactured on demand [2]. Another key benefit of additive manufacturing is the incredible geometric freedom that enables cost-effective fabrication of complex parts, whilst avoiding expensive tooling [3]. Furthermore, computational analysis methods can be used to reduce the steps required for part optimization, from part design to process parameter optimization, reducing the cost and environmental impact of process development. Despite the benefits, there are still many factors that limit the widespread uptake of additive manufacturing in existing industry production lines. Some examples of barriers to AM include the limited catalog of AM optimized materials, material costs, and poor suitability for large production volumes. To appeal to industry, AM methods must provide fast and accurate part fabrication to compete with conventional manufacturing capabilities. This research presents the high speed fabrication of alumina parts by stereolithography, utilizing computational analysis methods to reduce the steps required for process optimization.

Ceramic processing by AM is gaining popularity in research and industry for the fabrication of complex parts with high thermal resistance, corrosion resistance, and high hardness, for various applications such as biomedical implants, electronics, and structural parts [4–7]. However, the fabrication of ceramic parts by additive manufacturing faces

many challenges. Generally, these materials are characterized by very high melting points and low ductility, making processing from the molten state prohibitively difficult. Heat treatments must be carefully controlled to prevent formation of cracks and pores due to poor thermal durability, and the hard and brittle sintered ceramic parts are difficult and expensive to machine [8]. Consequently, powder processing has been a popular route for research and development of ceramic AM, particularly by lithography-based fabrication.

Stereolithography is a vat photopolymerization AM method that fabricates parts layer-by-layer through selective curing of a photosensitive resin. In ceramic stereolithography, fine ceramic particles are dispersed in a liquid photopolymer, e.g., acrylate or epoxy monomers, to form a photosensitive, thixotropic slurry. A UV laser scans single layer cross sections of 3D model data (Computer Aided Design, CAD) to selectively cure the slurry. As the slurry is cured, the solidified photopolymer joins the ceramic particles and forms the designed geometry into a "green" part. The green part is thermally post-processed to remove the polymer matrix and sinter the part to a dense ceramic component.

In recent years, ceramic processing by stereolithography has been reported using a 355 nm UV laser with a 50 µm spot size under conditions of 50–350 mW, and a maximum scan speed of 3000 mm/s for alumina [9], and 2000 mm/s for Yttria Stabilised Zirconia (YSZ) [10]. Wu et al. reported stereolithographic processing of Zirconia-Toughened Alumina (ZTA) to form a complex dentoid part with a high density close to 100%, and the results of mechanical testing were comparable to ZTA parts shaped by conventional methods [11]. ZTA processing has also been described using a similar stereolithography technique as described in this work [12]. Ceramic stereolithography was carried out using a laser power of 400 mW and a scan speed of 4000 mm/s to create specimens for mechanical testing. The parts were reported to have superior mechanical performance than traditionally molded ZTA, however, a long sintering schedule was described. Lithography based ceramic manufacturing has also been used to fabricate complex alumina parts such as gear wheels, turbine blades, and cellular structures [13]. A high fabrication speed of 6000 mm/s was reported for stereolithography of alumina ceramic using a 355 nm UV laser at 1.2 W in [14], however, a higher fabrication speed is not commonly reported in other publications.

Ceramic paste composition is an important consideration for stereolithography. The solid content of the paste has a significant impact on processability and part properties [15]. A solid loading of greater than 50% is recommended to prevent the cracking of parts during binder removal and reduce shrinkage during sintering [16]. A high solid loading is generally recommended for improved part density and mechanical performance, however, the effect of composition on paste rheology is an important consideration [17]. A high solid content may increase the paste viscosity to an extent that homogenous layer spreading cannot be achieved, or may change the paste rheology from thixotropic to dilatant [18]. A low solid content may reduce the paste viscosity whereby paste layers can no longer self-support and flow freely, reducing processability. The balance between solid content and viscosity is an important factor for ceramic stereolithography. In this research, ceramic paste composition was computationally modelled to predict the maximum solid loading of alumina particles in an acrylic resin matrix, to reduce the time and cost of experimental paste optimization.

Stereolithography processing conditions such as laser power, scan speed, and spot size, influence the extent of photopolymerization and therefore the curing depth and curing width [19]. A curing depth of 1.5 × the layer thickness is preferred to ensure sufficient inter-layer lamination. To achieve a dimensionally accurate part, the measurement of the curing width is required to define a suitable laser offset to account for over-curing. These parameters are affected by the scattering of laser radiation by the solid particles in the resin matrix, therefore material properties such as particle size distribution and refractive index are important [20,21]. Modelling of the paste material and optical analysis was used in this research to predict the curing behavior of the ceramic slurries, and to estimate suitable laser processing parameters to achieve sufficient curing depth.

2. Materials and Methods

2.1. Particle Dispersion Modelling and Optical Analysis

Computational simulations were used to identify a suitable paste composition and laser processing conditions for the stereolithography of alumina particles dispersed in an acrylic resin. The discrete element method (DEM) was used to analyze powder behavior and predict the maximum filling rate of solid particles in a resin matrix. EDEM (Altair, Troy, MI, USA) was used to simulate the distribution of spherical particles of Al_2O_3 according to the measured particle size distribution (Dv_{50} = 2.2 µm) (Figure 1). A cylindrical geometry of 100 µm height and 50 µm diameter was filled with the alumina particles using a gravitational acceleration of 9.8 m/s^2.

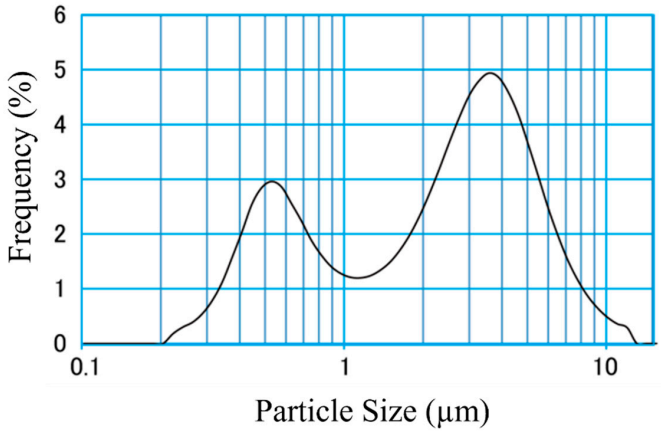

Figure 1. Particle size distribution of the Al_2O_3 powder material.

DEM was used to generate solid particles based on the physical properties of the alumina material, including the measured particle size distribution (Table 1). The rejection method and the local migration method were used to determine the position of the generated particles in the computation domain, removing instances where particles would overlap, and allowing solid particles to move randomly within a defined range. Particle contacts were calculated using a neighboring particle search, generating a collision determination lattice. Contact forces and external forces were calculated for the solid particles, and the sum of the forces was used to update particle position vector, velocity vector, and angular velocity vector, etc. The coordinate data of alumina particles in a cylindrical geometry of 50 µm diameter and 100 µm height was created. Particles were randomly generated within the cylinder and allowed to fall under gravity. Collisions and intermolecular forces were taken into account when particles were deposited into the cylinder, giving the number of particles and the maximum filling rate.

The calculated coordinate data from DEM simulations was used to generate a particle dispersion model. The model was further analyzed by ray tracing to assess the UV irradiance distribution from a 355 nm UV laser with a 50 µm spot size to represent the laser used in experimental investigations.

Table 1. Defined property values for alumina particle DEM simulations.

	Property	Value
Solid Particles and Solid Wall	Density (kg/m^3)	3850
	Poisson's Ratio	0.20
	Young's Modulus (GPa)	370
	Coefficient of Restitution	0.5
	Static Friction Coefficient	0.5
	Rolling Friction Coefficient	0.01
External Force	Gravitational Acceleration (m/s^2)	9.8

A cylindrical geometry of 50 μm diameter was created as the light source and the surface facing the particle dispersion model was defined as the ray emitting surface. The ray tracing software (LightTools, Synopsys Inc., Mountain View, CA, USA) used the coordinate and particle size data from the DEM analysis to populate a particle model for the analysis. Spheres were generated based on this data using a VBA (Visual Basic for Applications) macro. The optical properties of the light source, environment material, particle-free area between the light source and the observation plane, and solid particles, were defined (Table 2).

Table 2. Defined optical properties of the ray tracing analysis.

Element	Property	Value
Light Source	Wavelength (nm)	355
	Power (mW)	50–250
Environmental Material	Material	Acrylic
	Refractive Index	1.50
Solid Particles	Material	Alumina
	Refractive Index	1.75
	Transmittance (/m)	0.90
	Reflectance (%)	70

The observation plane was defined for ray tracing. Rays were assumed to be emitted perpendicular to the particle dispersion model, and the number of rays was defined as one million. The observation plane was created parallel to the emitted rays and positioned to vertically bisect the particle dispersion model with a square element (mesh) of 0.5 × 0.5 μm.

Photosensitive material is assumed to remain liquid until UV exposure (E, J/cm^2) reaches a critical exposure (E_c, J/cm^2). When laser exposure reaches E_c, the material reaches a "gelation point". At this point, the material solidifies. The UV exposure (E, J/cm^2) is expressed as a product of the UV irradiance (I, W/cm^2) and time (t, s) (Equation (1)).

$$E = I \times t, \tag{1}$$

Irradiance time was defined for a single instance of irradiation on an area (S, μm^2), using a defined laser spot diameter φ (μm), and scanning speed (V, μm/s) (Equation (2)).

$$t = \frac{S}{\varphi \times V} = \frac{\pi \times \left(\frac{\varphi}{2}\right)^2}{\varphi \times V} = \frac{\pi \varphi}{4V}, \tag{2}$$

Using RT analysis, the UV irradiance distribution in an arbitrary observation plane was obtained. The UV exposure (E, J/cm^2) was calculated at each coordinate (x, y, z). If the UV exposure was greater than or equal to the critical exposure (E_c), the point was considered cured (Equation (3)). The upper limit of scanning speed to achieve curing was then determined (Equation (4)).

$$I \times t \geq E_c \tag{3}$$

$$V \leq I \times \frac{\pi \varphi}{4E_c} \tag{4}$$

UV exposure was calculated and compared to the critical exposure for the photosensitive material to determine upper limits of scan speed to achieve material curing. The results of DEM and ray tracing analysis were used to predict the maximum filling rate of alumina particles in the photosensitive paste composition, and the optimum laser conditions, and compared with experimental values.

2.2. Paste Formation

A thixotropic paste was formed by dispersing ceramic particles within a photosensitive acrylic resin matrix. The maximum solid content and suitable processing conditions were predicted by the discrete element method (DEM) and ray tracing (RT) analysis. Alumina (Al_2O_3) particles of 2.2 µm average particle size (Sumitomo Chemical: AES-23) were weighed accordingly and combined with the photosensitive acrylic resin (JSR: KC1287). The material was thoroughly mixed and degassed by planetary centrifugal mixer (SK-350T, Shashin Kagaku, Kyoto, Japan). The simultaneous rotation and revolution ensured homogenous mixing and defoaming by centrifugal force (Figure 2). Mixing was carried out at 500 rpm rotation and 700 rpm revolution for three cycles of 5 min.

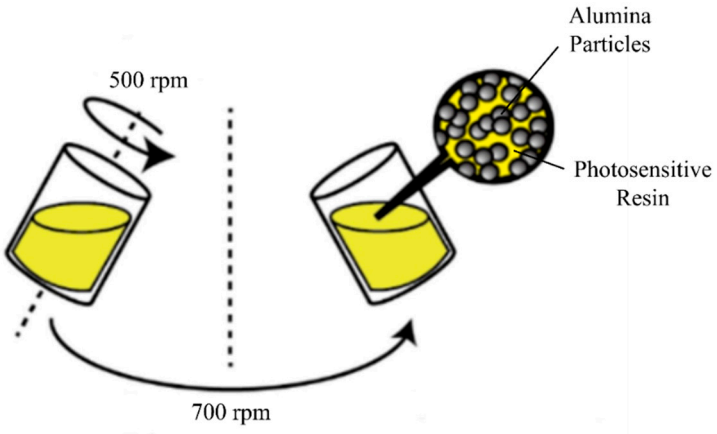

Figure 2. Schematic diagram of paste mixing by simultaneous rotation and revolution.

2.3. Stereolithographic Additive Manufacturing

Experimental investigations were carried out using a stereolithography system equipped with a 355 nm UV laser with a spot size diameter of 50 µm (SZ-2500, S.K. Fine, Kusatsu, Japan). Parts were fabricated on a plastic film of 50–75 µm thickness adhered to the 250 × 250 mm build platform. The paste material was deposited onto the build platform by automatic syringe and spread across the film by a blade to create a homogenous layer of a defined thickness. Single layer cross sections were solidified by UV laser radiation as directed by 3D model data (computer aided design, CAD). The process was repeated to build 3D parts layer-by-layer through material curing and inter-layer lamination (Figure 3).

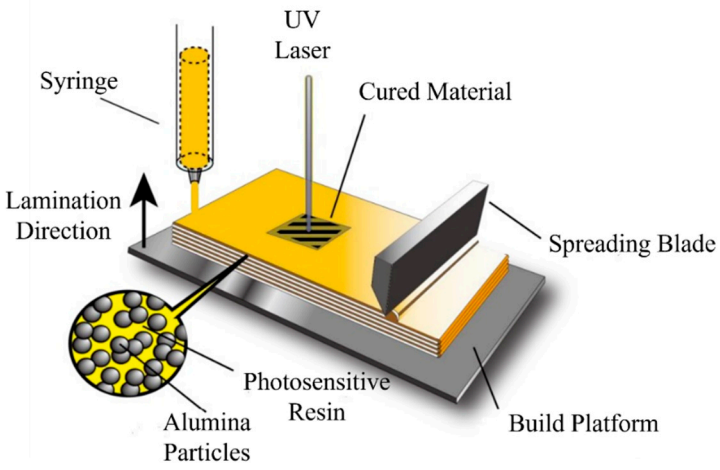

Figure 3. Schematic of the stereolithography process.

2.4. Parameter Investigation

Initial processing conditions were investigated to confirm optimal parameters for material consolidation by stereolithography. Laser power (mW), scan speed (mm/s), spot size (mm), and laser offset (mm), were altered and the effects on material consolidation observed. A test specimen was designed to measure the curing depth and laser over-cure for the formulated alumina slurry for specified laser power and scan speed combinations. The test specimen model was a thin film of two layers thickness, with a 1 mm diameter hole in the center (Figure 4). Laser processing of a single layer resulted in thin film specimens that were measured using digital optical microscopy. The measured film thickness was used to determine the curing depth associated with the laser parameters. Comparison of the designed and experimental hole diameter was used to determine the laser offset values, which allows compensation for excess material consolidation caused by ceramic particles reflecting the laser in the resin medium. The laser travel path was adjusted by the laser offset value to achieve precise dimensional fabrication.

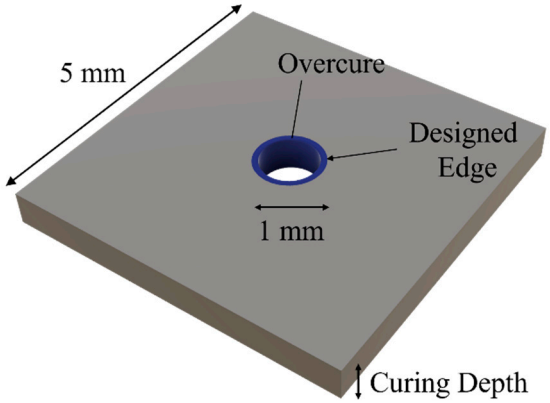

Figure 4. Test specimen of 5 × 5 mm with a 1 mm diameter hole in the center.

Complex specimens were designed and fabricated using the optimal parameters that were determined through computational and experimental investigations.

2.5. De-Binding and Sintering

The formed composite precursors were thermally treated to remove non-ceramic content and achieve a fully dense part by sintering (S7-2025D, Motoyama Corporation, Osaka, Japan) (Figure 5). For this process, composite "green" parts were heat treated at 600 °C and held isothermally for 2 h to remove uncured material. During this phase of the heat treatment, gas is released as a consequence of resin decomposition. To prevent parts from cracking or deforming, the heating rate was carefully controlled at 2.5 °C/min. After de-binding, the green parts were further heated for 2 h at a high temperature (1600 °C) to fully densify the ceramic, forming a polycrystalline body with controlled relative density and microstructure. Sintered density was measured by the Archimedes method.

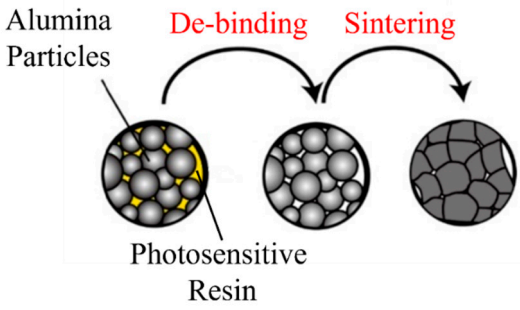

Figure 5. Schematic of thermal treatment process of stereolithography composite "green" parts.

3. Results and Discussion

3.1. Computational Analysis

3.1.1. Particle Dispersion Modelling and Ray Tracing Analysis

Particle dispersion models were created for alumina particles in an acrylic resin matrix. The predicted maximum particle packing ratio was 63.9 vol% (Figure 6). The illuminance distribution in the parallel observation plane obtained during RT analysis was used to visualize the curing aspect. The critical exposure (E_c) of the photosensitive acrylic resin was determined experimentally as 10 mJ/cm^2. A particle dispersion model was generated for alumina material in an acrylic resin matrix, using six defined particle sizes from the measured distribution. Optical analysis was used to predict the scanning speed required to achieve critical exposure at varying laser power using a 355 nm UV laser with a 50 µm spot size. The calculated values were used to visualize the curing depth of the UV irradiance under defined conditions (Figure 7).

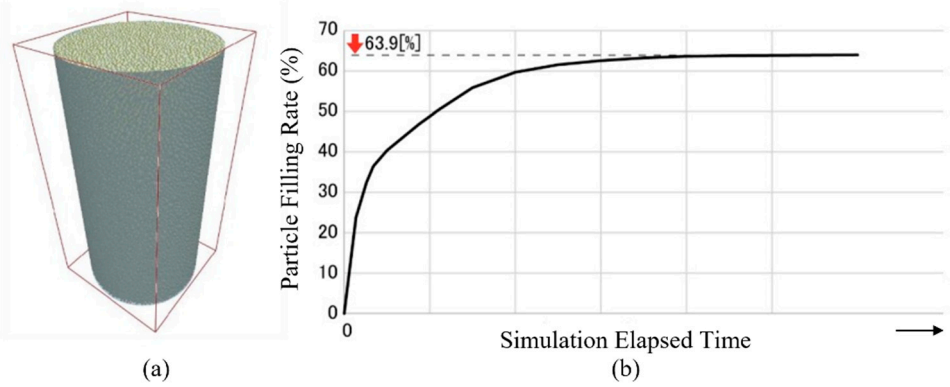

Figure 6. (**a**) Simulated DEM particle dispersion model, and (**b**) calculated particle filling rate.

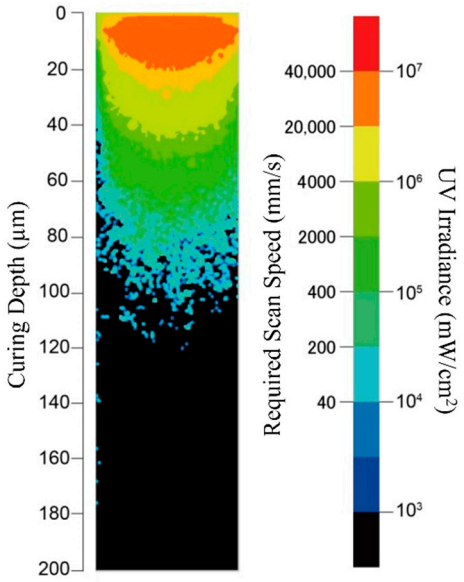

Figure 7. Ray tracing visualization of the curing depth of Al_2O_3 paste and the corresponding predicted values for required scan speed.

3.1.2. Paste Formulation and Stereolithography Processing

The maximum particle filling ratio as predicted by DEM (63.9%) was compared to experimental values. For the Al_2O_3 material used, a maximum solid loading of 65% was found. To ensure homogenous paste spreading in the stereolithography system, a reduced solid loading of 0–10% is recommended to ensure sufficient viscosity for practical

application. A suitable paste composition of 60–61.9% Al_2O_3 was determined and ensured satisfactory paste spreading.

Test specimens described in Section 2.5 were fabricated using the formulated paste with a laser power of 100 mW, a spot size of 50 µm, a laser offset of 0 µm, and scan speeds between 500–20,000 mm/s. The samples were measured by digital optical microscopy, using the sample thickness to determine curing depth, and the hole diameter to define a required laser offset for accurate processing. The curing depth measurements were compared to the computationally predicted values. A similar trend was found for the predicted and measured values; however, the predicted curing depths were 30–150 µm less than the measured values (Figure 8).

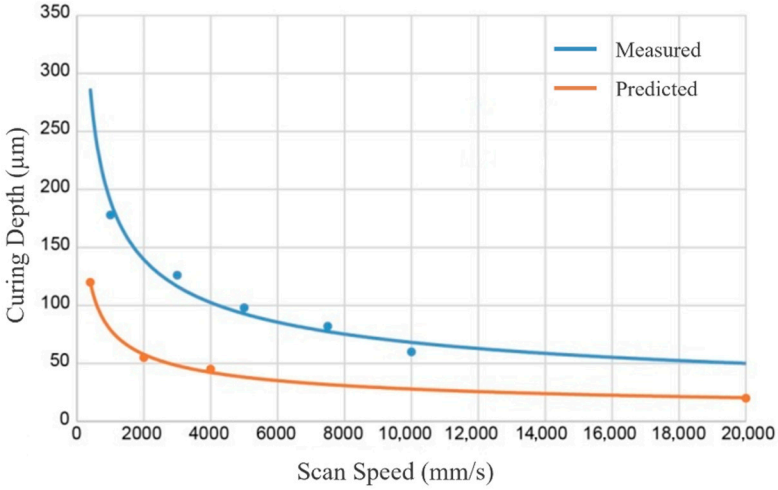

Figure 8. Measured and predicted values for curing depth and corresponding required scan speed for Al_2O_3 stereolithography.

One potential explanation for the increased experimental curing depth compared to the computational model is increased material irradiance due to the continuous operation of the laser during processing. The optical analysis assumed a single instance of laser irradiation in a given area, but during laser processing the laser radiation may be scattered, and material may be repeatedly irradiated to some degree, increasing the extent of material curing. Additionally, as the photosensitive material is cured, the refractive index is assumed to change, and this was not included in the computational model. Furthermore, the original optical analysis assumed solid particles were spherical, however, the actual morphology of the Al_2O_3 particles was irregular and angular. A second optical analysis was carried out using octahedral particles and the predicted curing depths were compared to the original spherical particle model (Figure 9). The models show greater curing depth in the octahedral particle model compared to the spherical particle model, suggesting that particle morphology effects the reflection and refraction of UV rays and therefore influences the curing depth. For accurate predictions, these factors should be taken into consideration during optical modelling.

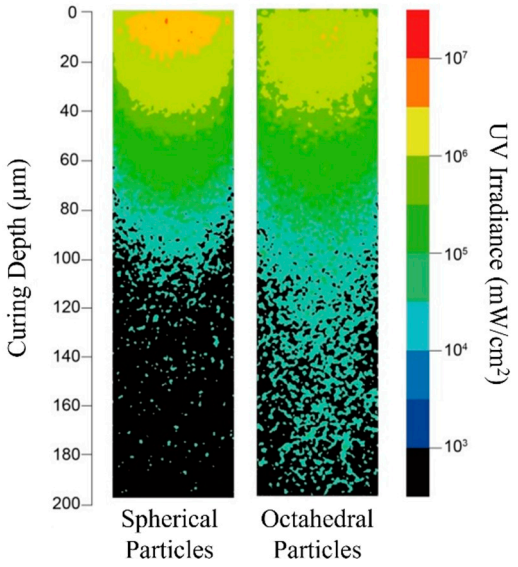

Figure 9. Ray tracing analysis of simulated Al_2O_3 pastes containing spherical or octahedral particles.

A hexagonal honeycomb structure was designed to demonstrate the potential application of high speed STL fabrication of an alumina thermoacoustic "stack" element (Figure 10). A cylindrical stack with a 2 cm radius and 5 cm height was designed with gradient flow path diameters from 1 to 1.5 mm. The structures were fabricated using the optimal paste composition (61.9% Al_2O_3) and processing parameters as previously described. Paste layers of 100 μm thickness were processed by a 355 nm UV laser with a spot size of 50 μm, using a laser power of 220 mW and a scan speed of 7500 mm/s. These parameters achieved a curing depth of 1.5 × the layer thickness. A laser offset of 200 μm was experimentally determined and used to reduce the dimensional error caused by excess curing adjacent to the laser scan path. The composite precursor was cleaned and thermally post-processed to de-bind and sinter as described in Section 2.5. A dense ceramic part was obtained with no observed cracking or porosity. Isotropic linear shrinkage of 13.5% and a sintered density of 99.3% was measured.

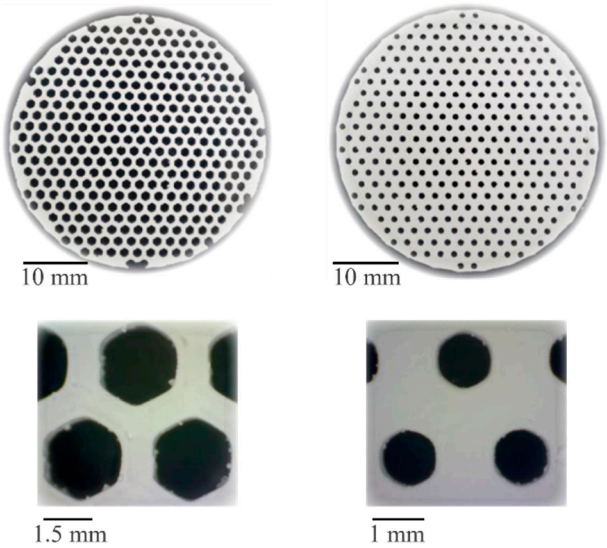

Figure 10. Complex honeycomb "stack" structure with gradient flow channels fabricated by high-speed alumina stereolithography.

4. Conclusions

Computational simulations were used to simulate the behavior of alumina particles in a photosensitive resin matrix and predict suitable material composition and laser processing parameters. The computational models were used to inform stereolithographic processing of the alumina paste material and reduced the number of experimental iterations required to optimize processing. The predicted maximum solid content of alumina particles in the paste material was experimentally validated and 61.9 vol% alumina was used for experimental paste composition. Suitable laser processing conditions were informed by ray tracing analysis through the prediction of curing depth corresponding to laser irradiance. The trend in curing depth with laser irradiance was successfully predicted by optical analysis, with the difference in experimental values thought to be caused by particle morphology.

High-speed fabrication of a complex alumina thermoacoustic "stack" element was demonstrated using the optimized processing conditions as predicted by the computational simulations. In these experiments, a scan speed of 7500 mm/s was used to process the alumina material.

Author Contributions: Conceptualization, S.K. and T.I.; methodology, T.I.; software, T.I.; validation, T.I., S.K., and F.S.; formal analysis, T.I.; investigation, T.I.; resources, S.K.; data curation, T.I.; writing—original draft preparation, F.S.; writing—review and editing, F.S.; visualization, F.S.; supervision, S.K.; project administration, S.K.; funding acquisition, S.K. All authors have read and agreed to the published version of the manuscript.

Funding: This research received no external funding.

Data Availability Statement: Not applicable.

Conflicts of Interest: The authors declare no conflict of interest.

References

1. Gibson, I.; Rosen, D.; Stucker, B. *Additive Manufacturing Technologies*, 2nd ed.; Springer: New York, NY, USA, 2015.
2. Ford, S.; Despeisse, M. Additive Manufacturing and Sustainability: An Exploratory Study of the Advantages and Challenges. *J. Clean. Prod.* **2016**, *137*, 1573–1587. [CrossRef]
3. Halloran, J.W. Ceramic Stereolithography: Additive Manufacturing for Ceramics by Photopolymerization. *Annu. Rev. Mater. Res.* **2016**, *46*, 19–40. [CrossRef]
4. Felzmann, R.; Gruber, S.; Mitteramskogler, G.; Tesavibul, P.; Boccaccini, A.R.; Liska, R.; Stampfl, J. Lithography-Based Additive Manufacturing of Cellular Ceramic Structures. *Adv. Eng. Mater.* **2012**, *14*, 1052–1058. [CrossRef]
5. Du, X.; Fu, S.; Zhu, Y. 3D Printing of Ceramic-Based Scaffolds for Bone Tissue Engineering: An Overview. *J. Mater. Chem. B* **2018**, *6*, 4397–4412. [CrossRef] [PubMed]
6. Zocca, A.; Colombo, P.; Gomes, C.M.; Günster, J. Additive Manufacturing of Ceramics: Issues, Potentialities, and Opportunities. *J. Am. Ceram. Soc.* **2015**, *98*, 1983–2001. [CrossRef]
7. Bae, C.J.; Ramachandran, A.; Chung, K.; Park, S. Ceramic Stereolithography: Additive Manufacturing for 3D Complex Ceramic Structures. *J. Korean Ceram. Soc.* **2017**, *54*, 470–477. [CrossRef]
8. Lakhdar, Y.; Tuck, C.; Binner, J.; Terry, A.; Goodridge, R. Additive Manufacturing of Advanced Ceramic Materials. *Prog. Mater. Sci.* **2021**, *116*, 100736. [CrossRef]
9. Kirihara, S. Systematic Compounding of Ceramic Pastes in Stereolithographic Additive Manufacturing. *Materials* **2021**, *14*, 7090. [CrossRef] [PubMed]
10. Takahashi, M.; Kirihara, S. Stereolithographic Additive Manufacturing of Zirconia Electrodes with Dendritic Patterns for Aluminum Smelting. *Appl. Sci.* **2021**, *11*, 8168. [CrossRef]
11. Wu, H.; Liu, W.; He, R.; Wu, Z.; Jiang, Q.; Song, X.; Chen, Y.; Cheng, L.; Wu, S. Fabrication of Dense Zirconia-Toughened Alumina Ceramics through a Stereolithography-Based Additive Manufacturing. *Ceram. Int.* **2017**, *43*, 968–972. [CrossRef]
12. Li, M.; Liu, W.; Nie, J.; Wang, C.; Li, W.; Xing, Z. Influence of Yttria-Stabilized Zirconia Content on Rheological Behavior and Mechanical Properties of Zirconia-Toughened Alumina Fabricated by Paste-Based Stereolithography. *J. Mater. Sci.* **2021**, *56*, 2887–2899. [CrossRef]
13. Schwentenwein, M.; Homa, J. Additive Manufacturing of Dense Alumina Ceramics. *Int. J. Appl. Ceram. Technol.* **2015**, *12*, 1–7. [CrossRef]
14. Chen, S.; Wang, C.-S.; Zheng, W.; Wu, J.-M.; Yan, C.-Z.; Shi, Y.-S. Effects of Particle Size Distribution and Sintering Temperature on Properties of Alumina Mold Material Prepared by Stereolithography. *Ceram. Int.* **2022**, *48*, 6069–6077. [CrossRef]
15. Liu, W.; Li, M.; Nie, J.; Wang, C.; Li, W.; Xing, Z. Synergy of Solid Loading and Printability of Ceramic Paste for Optimized Properties of Alumina via Stereolithography-Based 3D Printing. *J. Mater. Res. Technol.* **2020**, *9*, 11476–11483. [CrossRef]

16. Brady, A.; Grumman, N.; Chu, T.-M.G.; Halloran, J.W. Curing Behavior of Ceramic Resin for Stereolithography. In *International Solid Freeform Fabrication Symposium*; The University of Texas: Austin, TX, USA, 1996.
17. Doreau, F.; Chaput, C.; Chartier, T. Stereolithography for Manufacturing Ceramic Parts. *Adv. Eng. Mater.* **2000**, *2*, 493–496. [CrossRef]
18. Sigmund, W.M.; Bell, N.S.; Bergström, L. Novel Powder-Processing Methods for Advanced Ceramics. *J. Am. Ceram. Soc.* **2004**, *83*, 1557–1574. [CrossRef]
19. Chartier, T.; Chaput, C.; Doreau, F.; Loiseau, M. Stereolithography of Structural Complex Ceramic Parts. *J. Mater. Sci.* **2002**, *37*, 3141–3147. [CrossRef]
20. Xing, H.; Zou, B.; Liu, X.; Wang, X.; Chen, Q.; Fu, X.; Li, Y. Effect of Particle Size Distribution on the Preparation of ZTA Ceramic Paste Applying for Stereolithography 3D Printing. *Powder Technol.* **2020**, *359*, 314–322. [CrossRef]
21. Sun, C.; Zhang, X. The Influences of the Material Properties on Ceramic Micro-Stereolithography. *Sens. Actuators A Phys.* **2002**, *101*, 364–370. [CrossRef]